

# Dry-Released Nanotubes and Nanoengines by Particle-Assisted Rolling

Jinxing Li, Jing Zhang, Wei Gao, Gaoshan Huang, Zengfeng Di, Ran Liu,\* Joseph Wang, and Yongfeng Mei\*

Slender structures in nature, for example, from leaves, petals to proteins and DNA, usually tend to fold or roll into diverse three-dimensional configurations. Beyond changing the size and form, folding and rolling can transform relatively simple structures into complex shapes with new and distinct properties. Mimicking these naturally occurring assembly processes by thinning, shaping, and rolling artificial free sheets can be implemented to create novel 3D fine structures and devices at small scales.<sup>[1–5]</sup> A sheet of paper can be easily rolled up by external force, while the rolling of a nanomembrane (a thin solid film with thickness below 100 nm),<sup>[1,2]</sup> is usually driven by internal strain.<sup>[6]</sup> Such 3D nanomembranes, with combination of low-dimensional characteristics and unique mechanical features, are well documented as innovate building blocks in, for example, flexible electronics,<sup>[7]</sup> energy storage,<sup>[8]</sup> optical resonators and metamaterial fibers,<sup>[9,10]</sup> microfluidics,<sup>[11]</sup> biosensors,<sup>[12]</sup> and self-propelled micromachines.<sup>[13,14]</sup> However, the scalability of strain-engineered 3D structures is still constrained by the magnitude of intrinsic stress that can be built in the nanomembranes. Moreover, the stress releasing process for the rolling of nanomembranes always involves a sacrificially wet etching, which tends to bring damages to the fabricated fine structures and complexity for processing. Furthermore, it is still challenging but extremely attracting to build hybrid 3D nanostructures with tailored surface chemistry and nano-topography.

Here, we demonstrate a dry-releasing approach to roll up nanomembranes into micro-/nanotubes by burning of sacrificial layers. With the assistance of dewetted nanoparticles,

surface tension of metal droplets can drive the radii of rolled-up tubes into nanometer scale with ultrahigh aspect ratio. Similar to chaperones fold proteins with functional biological properties,<sup>[15]</sup> a large loading of Pt nanoparticles with tailored sizes and distributions in the walls enable such nanoengines made of rolled-up nanotubes working as high-speed catalytic nanoengines in a fuel solution. Compared to normal catalytic tubular nanoengines (based on an inner continuous Pt film), the nanoparticle-coated nanoengines exhibit a four-fold acceleration due to their large specific surface areas and enhanced mass transfer of the peroxide fuel toward the catalytic Pt nanoparticles, analogous to the behavior of nanoelectrode arrays/ensembles.<sup>[16]</sup> Our results also indicate that guided rolling and folding a thin substrate can allow a reproducible construction of functionalized complex and fine structures.

Generally, in order to fold or roll a sheet on a support, energy minimization or strain release, which could be extrinsic or intrinsic, is required to bend the flat structure out of the plane. At macro or millimeter scale, active actuations such as pneumatics,<sup>[17]</sup> magnetic forces,<sup>[18]</sup> thermal treatment,<sup>[19]</sup> and bio muscular actuation<sup>[20]</sup> are straight forward to curve films with mill- to micrometer scale radii (case I in **Figure 1a**). When the sheet is thinning down to the nanometer scale, its bending behavior sensitively depends on the built-in strain gradient across the film thickness. Structure deformation triggered by the intrinsic strain can be deterministically engineered for 3D nanomembrane production (case II in **Figure 1a**).<sup>[21,22]</sup> An example of strain-engineered SiO/SiO<sub>2</sub> microtube is displayed in the **Figure 1b**. In this case, built-in strain in a bilayer is mainly created by their different thermal expansion properties or lattice mismatch using conventional deposition methods. Due to the limitation of intrinsic strain that can be built, rolled-up tubes with small radii at nanoscale are still challenging for such strain-engineered self-assembly. Additionally, a couple of issues associated with strain releasing processes, such as wet-etching and capillary induced adhesion, usually tend to bring defects and damages to the suspended 3D nanostructures and render the devices useless. On the other hand, as solid films get thinner, surface-induced forces like surface tension of metal droplets become dominant and are expected to play an important role in determining the curvature of nanomembranes.<sup>[23,24]</sup> Alternatively, it is anticipated that the wetting interaction of nanodroplets can be used to tailor the shape of nanostructures. Our approach is taking advantages of the surface tension of metal nano-droplets (i.e., particles when cooling down) associated with the built-in strain in nanomembranes (case III in **Figure 1a**), and thus, this new type of self-rolling driven by the

J. X. Li, J. Zhang, Prof. G. S. Huang, Prof. Y. F. Mei  
Department of Materials Science  
Fudan University  
Shanghai 200433, China  
E-mail: yfm@fudan.edu.cn

J. X. Li, J. Zhang, Prof. R. Liu  
State Key Lab of ASIC and System  
Fudan University  
Shanghai 200433, China  
E-mail: rliu@fudan.edu.cn

W. Gao, Prof. J. Wang  
Department of Nanoengineering  
University of California-San Diego  
La Jolla, CA 92093, USA

Prof. Z. F. Di  
State Key Laboratory of Functional Materials for Informatics  
Shanghai Institute of Microsystem and Information Technology  
Chinese Academy of Sciences, Shanghai 200050, China



DOI: 10.1002/adma.201301208

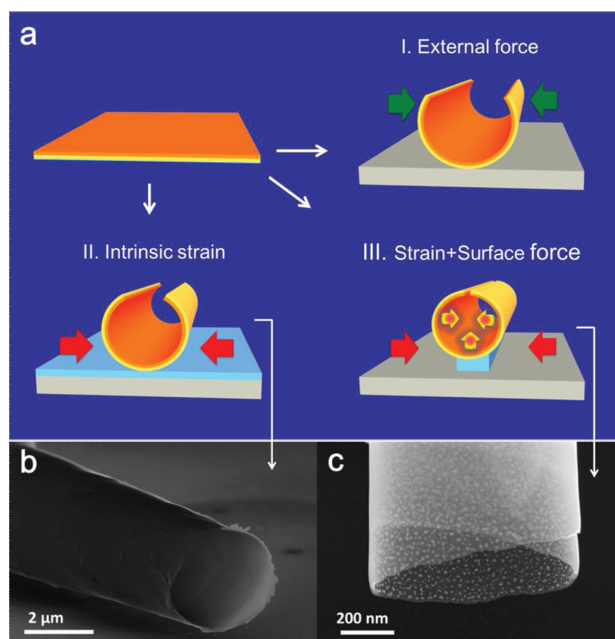


**Figure 1.** Methodologies for flat sheet rolling via different driving forces. a) Schematic of the rolling driving forces: I) at macro and microscale, rolling up by external force; II) at micro-/nanoscale, rolling up by intrinsic strain; III) at nanoscale, rolling by strain and surface forces. b) A SEM image of a strain-engineered SiO/SiO<sub>2</sub> microtube with an initial nanomembrane thickness of 10/10 nm and c) a SEM image of a particle-assisted rolled-up SiO/SiO<sub>2</sub> nanotube with an initial nanomembrane thickness of 10/10 nm.

cooperation of strain relaxation and surface force is utilized to create extremely nanoscale rolled-up tubes (i.e., nanotubes) from flat nanomembranes. As one can see the scanning electron microscopy (SEM) image in Figure 1c, with the same nanomembrane thickness (20 nm) of the microtube in Figure 1b, a SiO/SiO<sub>2</sub> nanotube with diameter of ≈800 nm is rolled up here, where the inner surface of the nanotube is coated with Au nanoparticles. The wetting interactions between these nanoparticles working as nanodroplets and nanomembranes during thermal annealing process bring a considerable surface tension for their rolling, and hence overcome the deformation limit to get very small radius of rolled-up nanotubes.

As displayed in Figure 2a, we firstly deposit a thin metal layer (<10 nm, labeled as yellow) on the top surface of pre-stained bilayered nanomembrane (labeled blue and violet), while the underneath PMMA polymer is used as a sacrificial layer (not displayed here). The sample was then treated by rapid thermal annealing (RTA) in N<sub>2</sub> environment to trigger the dewetting of the gold layer. This thermal dewetting process starts from stretching the liquid gold film to separated islands, responding to the surface tension between the metal nanodroplets and the nanomembrane. Simultaneously, the nanomembrane was released from the support due to the burning of PMMA in this annealing process. During this thermal releasing and dewetting process, the surface tension of the nanoparticles and the nanomembrane rolling. Consequently, we can achieve rolled-up nanotubes with nanoscale diameters

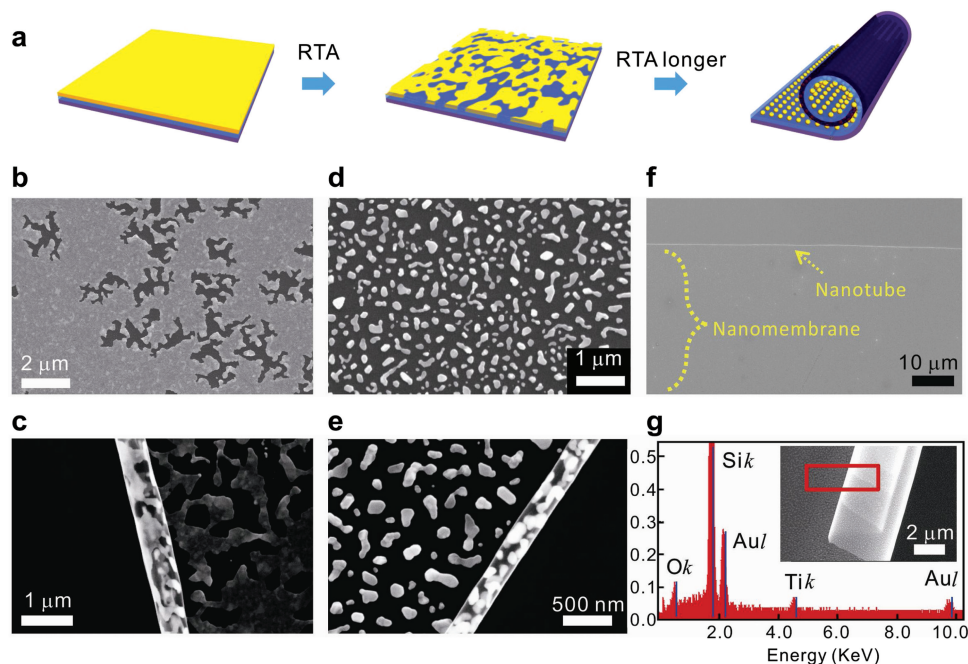


**Figure 2.** Particle-assisted rolling process. a) Schematic illustration of nanodroplets formation process and nanomembrane rolling upon a thermal dewetting treatment. b) Surface morphology of nanomembrane and c) rolled-up SiO/SiO<sub>2</sub> (5/5 nm) nanotube after thermal dewetting of the upper gold layer at 500 °C for 10 s. The Au film became discontinuous during the thermal dewetting. d) Surface morphology and e) rolled-up SiO/SiO<sub>2</sub> (5/5 nm) nanotube after thermal dewetting of the upper gold layer at 500 °C for 30 s. An array of gold nanoparticles were thermodynamically self-assembled with longer dewetting time. The nanoparticle-decorated nanomembrane can roll up into nanotube with a diameter of ≈300 nm. The gold nanoparticles on the nanomembrane are enclosed in the tube shell. f) SEM image of a long rolled-up nanotube released from SiO/SiO<sub>2</sub> nanomembrane with gold nanoparticles. g) Energy dispersive X-ray spectrum analysis on a Au nanoparticle-coated tube displayed in the inset SEM image.

decorated with self-assembled gold nanoparticles, whose size can be tuned by the annealing time and temperature.

This process was exemplified by annealing the SiO/SiO<sub>2</sub>/Au (5/5/3 nm) nanomembrane at 500 °C for 10 s and 30 s. The surface morphology of the flat nanomembrane and corresponding rolled-up nanotubes are shown in Figure 2b,c (annealed for 10 s) and Figure 2d,e (annealed for 30 s). After annealing for 10 s, the gold film becomes discontinuous and the nanoislands with irregular shape are formed on the surface of nanomembranes. Meanwhile, the nanomembranes are rolled up into nanotubes with a diameter of ≈600 nm and the gold nanoislands are enclosed in the tube. Figure 2d,e clearly shows that the gold film is ruptured into nanoparticles when the annealing time was increased from 10 s to 30 s. The nanotubes formed here have a diameter of ≈300 nm, which is only ≈3 times larger than the diameter of the Au nanoparticles enclosed in the tube walls. A uniform and long Au nanoparticle-coated SiO/SiO<sub>2</sub> nanotube is displayed in Figure 2f. The nanotube can reach a length of almost one centimeter and still hold a good uniformity in diameter (≈200 nm). In Figure 2g, energy dispersive X-ray (EDX) spectrum analysis results of released nanomembranes demonstrate the presence of gold nanoparticles and the absence of carbon, which indicates that the PMMA is completely removed by the rapid thermal annealing (i.e., burning in a very dilute oxygen gas in N<sub>2</sub> environment). Importantly, a significant advantage of this approach is using a single-step dry process without wet etching to release strained layers and subsequent rinsing, which thus prevents the released micro or nanostructures from sticking on substrates and collapse by themselves due to the liquids inside the tubes.

It is known that noble metal nanoparticles, especially for gold, silver, and platinum, exhibit unique physical and chemical properties such as localized plasmon resonance and high catalytic activity. To demonstrate the generalization of this particle-assisted rolling approach, rolled-up SiO/TiO<sub>2</sub> nanomembranes coated with a series of noble metal layers are presented in **Figure 3**: a) gold nanoparticles, b) silver nanoparticles, c) gold/silver alloy nanoislands, d) platinum nanoparticles. It is found that while a single metal layer tends to form nanoparticle array after thermal dewetting, the alloy metal layer usually prefers to form a nanoporous network, as displayed in Figure 3c. The surface morphology of the nanotube can be also modified by choosing different metal layer thickness, dewetting time and temperature. To achieve their radii down to 100–1000 nm is challenging under an equal thickness if only using their intrinsic strain, no matter in highly stressed metal films such as chromium whose tensile stress can be up to 1.6 GPa,<sup>[25]</sup> or epitaxial semiconductor layers grown by molecular beam epitaxy (MBE) method.<sup>[26]</sup> As far as we know, it is hard to get rolled-up oxide tubes with diameter below one micrometer based on normal evaporation deposition methods, although atomic layer deposition can do it but only with a layer thickness of two monolayers. A transmission electron microscope (TEM) image of a Pt nanoparticle-coated nanotube is shown in Figure 3e. It is obvious that the tube with one rotation reveals Pt nanoparticles with uniform size (around 30 nm, left image), while that with two or more rotations presents overlap of the particles in the walls (right image), which implies the excellent capability of loading functional particles. Besides, our particle-coated

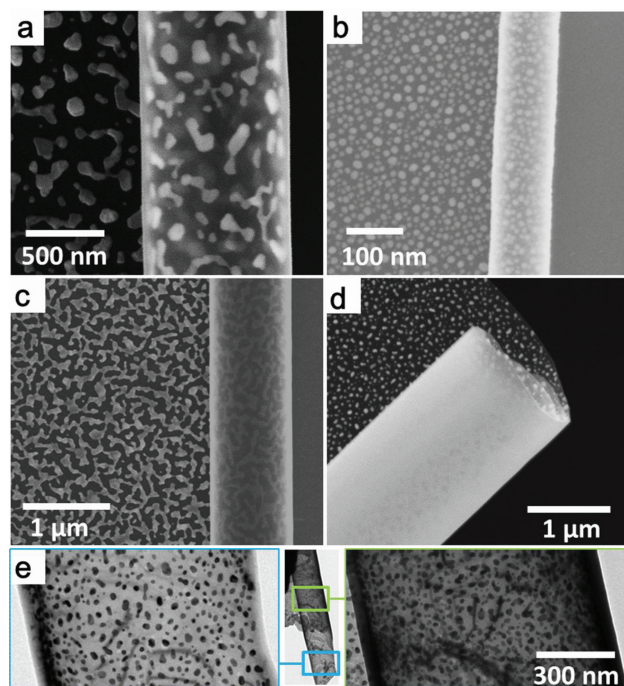


**Figure 3.** Particle-assisted rolling of micro-/nanotubes based on different nanoparticles. SEM images of micro-/nanotube coated with a) gold nanoparticles, b) silver nanoparticles, c) gold/silver alloy nanoislands, and d) platinum nanoparticles. e) The middle image shows a TEM image of a Pt nanoparticle-coated nanotube, while the left one reveals the TEM image of the tube with one rotation and the right one is the TEM image of the tube with two rotations.

nanotubes are featured with better uniformity and large length-diameter ratio (up to 10<sup>5</sup>), which is quite adaptable as candidates for nanofluidics channels as well.

Tailoring and scaling of 3D nanostructures self-assembly need a precise control of the forces at nanoscale. Our interest in the nanoparticle-assisted assembly process was provoked by the finding that these dewetting metal nanoparticles confined in large nanomembranes also exhibit surface stress and do compress nanotubes with very small radii. To explain the rolling process and identify its governing parameters, a mechanical model has been developed here. When a flat thin film is completely covered by a large droplet, the surface tension of the droplet bends the film and the film starts to wraps up into a 3D capillary-induced origami.<sup>[27]</sup> However, due to the competition between capillary force and bending barriers, the wrapping of thin films can take place only when the volume of the droplet is larger than a critical value.<sup>[28,29]</sup> Recently, the molecular dynamics simulations theoretically predict that a nanodroplet can guide and activate graphene folding but is only feasible for graphenes with several nanometers size.<sup>[30]</sup> Nevertheless, it is valuable to note that, though it is unable to fold or wrap a large film by a small droplet, the surface tension of a droplet still bring localized elastic deformation of a flexible thin film.<sup>[31]</sup> When the thin film is covered by a considerable number of nanodroplets, the resultant surface tensions of these nanodroplets would properly contribute to the thin film deformation, as demonstrated here.

Qualitatively, during nanomembrane releasing and nanoparticle dewetting, the increase of elastic energy due to rolling is balanced by the nanodroplets surface energy and initial strain relaxation. The competition among the surface tension  $\gamma$ , the initial bilayer strain difference  $\Delta\varepsilon$  and the bending stiffness  $D$  is supposed to determine the final shape of the nanomembrane after rolling transition. Consider a flat nanomembrane, as illustrated in a two-dimensional model in Figure 4a, the energy required to bend it out of a plane is related to its rigidity. According to the theory of elasticity,<sup>[32]</sup> the bending energy is

$$E_B = \frac{D}{2} \int \left( \frac{1}{R} - \frac{1}{R_0} \right)^2 dA \quad (1)$$

Where  $D = B h^3 / [12 (1 - \nu^2)]$  is the bending stiffness,  $B$  is the Young's modulus, with  $\nu$  the Poisson's ratio and  $h$  the nanomembrane total thickness. During the thermal annealing, the elastic energy built in the nanomembrane is released and the resulted bending moment per unit width of the nanomembrane is  $M_S = (1 + \nu) D \Delta\varepsilon / h$ . To examine the rolling behavior of a nanomembrane coated with nanodroplets, one need to know the capillary force produced by all the nanodroplets. For a single nanodroplet, the capillary torque due to the surface tension  $\gamma$  and Laplace pressure  $P$  along the rolling line is  $M_C = 2\gamma \sin\theta R_d^2/3$ .<sup>[28]</sup> Assuming that all the nanodroplets on the nanomembrane are with the same radius  $R_d$  and contact angle  $\theta$ , for a given particle density per unit area  $n$ , the total capillary torque of all the nanodroplets is  $M'_C = n^{1/2} 2\gamma \sin\theta R_d^2/3$  in a 2D equilibrium state. Here we define a dimensionless number  $\alpha = M'_C / M_S$ , which describes the bending contribution of the nanodroplets-induced capillary torques comparing to the bending moment of the intrinsic strain. At a critical position after rolling up, the energy change due to strain relaxation and the capillary force is

$$\int \frac{M_S^2 + nM_C^2}{2D} dA = E_B \quad (2)$$

Thus the final tube curvature radius will be expressed as

$$R = \frac{1}{\sqrt{\alpha^2 + 1}} \frac{h}{(1 + \nu)\Delta\varepsilon} \quad (3)$$

which is relative to the nanoparticle properties and the nanomembrane parameters. The contour plot of Figure 4b shows the scaling law of the nanoparticle-assisted nanomembrane rolling, in terms of the SiO/TiO<sub>2</sub> (3/3 nm) tube radius as a function of the Ag nanoparticle size and density. Here, the boundary condition  $n\pi R_d^2 < 1$  gives the smallest tube can be obtained by this approach. Such mechanical model predicts that small tubes with radius smaller than 100 nm can be obtained with the assistance of the surface stressing from nanoparticles. The inset in Figure 4b shows the maps of SiO/TiO<sub>2</sub> tube rolling radius as functions of three different total thickness of nanomembrane  $h$ , with varying nanoparticle size  $R_d$  and density  $n$ . As expected, at a smaller nanomembrane thickness  $h$ , the radius of curvature exhibits a much stronger dependence of particle properties.

According to our theoretical prediction, we quantitatively demonstrate the scalability of particle-assisted rolling with

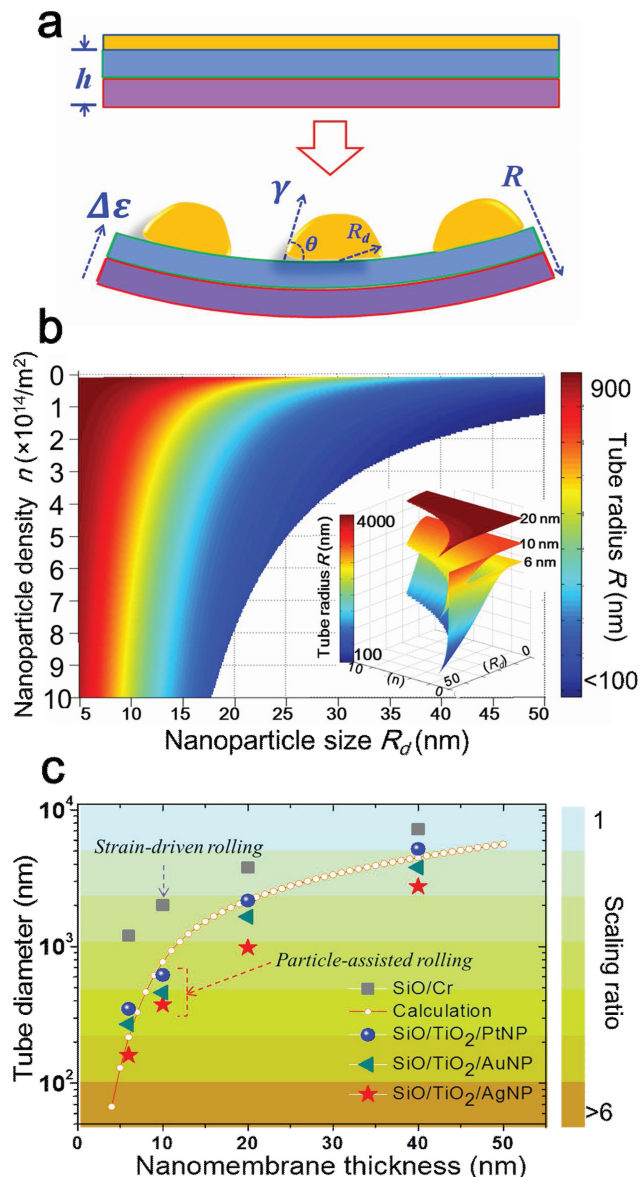


**Figure 4.** Scalability of nanotubes by particle-assisted rolling. a) Schematic diagram for the 2D equivalence of a curved nanomembrane due to competition of the surface tension of nanodroplets, the built-in strain, and the bending rigidity of nanomembranes. b) Theoretical estimation of SiO/TiO<sub>2</sub> (3/3 nm) tube radius as a function of the Ag nanoparticle (i.e., size and density). The inset displays the map of rolling radius as a function of a total thickness  $h$  (6–20 nm) of SiO/TiO<sub>2</sub> nanomembranes, with various nanoparticle size  $R_d$  (0–50 nm) and density  $n$  (0.1–10 × 10<sup>14</sup> m<sup>-2</sup>). c) Experimental results of the diameter of SiO/TiO<sub>2</sub> with various noble metal nanoparticles compared to those of normal strain-engineered microtubes without nanoparticles. Solid line is an approximate prediction based on our measured particle parameters and simple model (see the text). The color mapping indicates the particle-assisted scaling ratio  $(\alpha^2 + 1)^{1/2}$ .

various metal nanoparticles and different thickness, while strain-engineered microtubes released by thermal delamination without the thermal dewetting of metal layers are also prepared for reference. Two mostly stressed materials SiO and

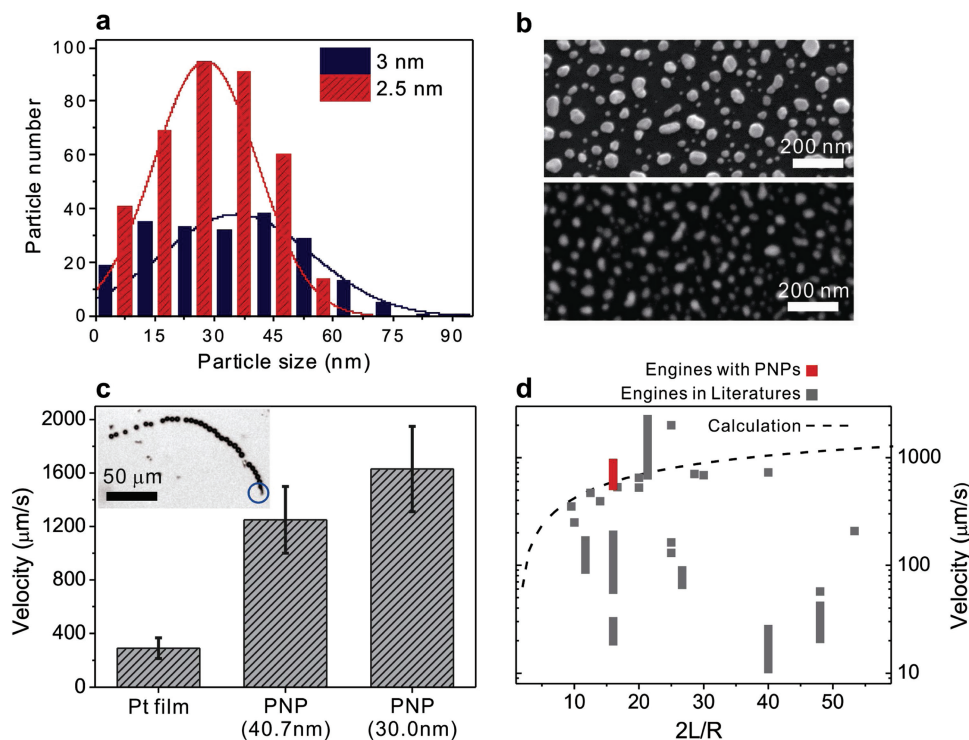


**Figure 5.** Superfast catalytic nanoengines coated with Pt nanoparticles. a) Pt nanoparticle size distribution on released SiO/TiO<sub>2</sub>/Pt nanomembrane with initial Pt thicknesses of 2.5 nm and 3 nm in an area of 1.6 μm<sup>2</sup>. b) Corresponding SEM images of the Pt nanoparticles with different sizes and distributions (upper to 2.5 nm and down to 3 nm). c) The statistic average speed of micro-/nanoengines with different inner layers in 10% H<sub>2</sub>O<sub>2</sub> aqueous solution: smooth Pt film, Pt nanoparticles (PNP) with mean size of 40.7 nm and Pt nanoparticles with mean size of 30.0 nm. The inset is a snapshot image of a fastest-moving microengine (speed: around 195 body lengths per second) coated with Pt nanoparticles in a 10% H<sub>2</sub>O<sub>2</sub> aqueous solution. d) The dependence of the speed of tubular engines on the tube geometry (2 L/R) in a 5% H<sub>2</sub>O<sub>2</sub> aqueous solution (normalized) at room temperature: this work (red column) and typical experimental data (grey squares and columns) extracted from literature.<sup>[35–45]</sup> The dashed line is a theoretical data based on Equation 5.

Cr, were chosen here for comparison. The preparation details and scalability of strain-engineered SiO/Cr microtubes are included in the Supporting Information. The inner diameter of nanoparticle-coated SiO/TiO<sub>2</sub> tubes, as well as strain-engineered tubes without particles, are shown in Figure 4c, associated with an approximate theoretical curve calculated from our experimental nanoparticle parameters. The particle-assisted scaling ratio  $(\alpha^2 + 1)^{1/2}$  which is defined by the tube radius ratio of tubes without nanoparticles and with nanoparticles, is also indicated by the color mapping here. From our experimental results, the diameter of the particle-coated tubes rolling from 6 nm nanomembrane is  $\approx 7$  times smaller than those strain-engineered tubes without particles. Due to the strong dependence of the nanomembrane stiffness on thickness, the surface force of the nanoparticle is becoming dominated over built-in strain when reducing the nanomembrane thickness. Differing from capillary wrapping by a large droplet, our results indicate that the surface forces produced by the nanodroplet group play a critical role in deterministic nanomembrane assembly. This effect is quite promising for deterministic self-folding and rolling of 2D materials, such as organic monolayers, carbon nanosheets and semiconductor nanomembranes.

The nanoparticles enclosed in the tubular structures with excellent physical and chemical properties may lead to a

dramatical enhancement of the device performance based on 3D nanomembrane. We demonstrate that the rolled-up nanotubes integrated with Pt nanoparticles show great potential in powerful catalytic nanoengines, with its large surface and ultra-small size. Catalytic micro-/nanoengines can self-propel by consuming chemical fuels and perform complex tasks, such as dynamic tiny cargo transportation and separation,<sup>[33,34]</sup> by catalytic decomposition of chemical fuels, for example, hydrogen peroxide (H<sub>2</sub>O<sub>2</sub>). Powerful micro-/nanoscale engines moving with fast speed and strong self-generated force are quite essential for their performance in drug delivery and environmental applications.<sup>[13,35]</sup>

Applying the above particle-assisted rolling, Pt-nanoparticle-coated nanotubes are fabricated to work as nanoengines. Figure 5a shows the size distribution of dewetted Pt nanoparticle attached on SiO/TiO<sub>2</sub>/Pt (SiO/TiO<sub>2</sub>, 5/5 nm in thickness) nanotubes with an initial Pt thickness of 2.5 nm and 3 nm. A Gaussian profile was used to fit to the size distribution of the nanoparticles. It is found that the mean Pt particle sizes are of 30.0 and 40.7 nm for the initial Pt thicknesses of 2.5 nm and 3 nm, respectively. The calculated nanoparticle densities are  $2.24 \times 10^{14} \text{ m}^{-2}$  and  $1.07 \times 10^{14} \text{ m}^{-2}$ , while their SEM images are displayed in the down and upper parts of Figure 5b. The thinner the initial Pt layer, the smaller the particle sizes, while

the higher the island density that are formed. Similar results are also observed for Au and Ag nanoparticle-coated nanomembranes. As stated above, the annealing process at different temperatures is an effective approach to tailor the sizes and densities of the nanoparticles which may modify catalytic properties of the rolled-up nanomembranes. Figure 5c displays average speeds of Pt-nanoparticle-coated nanoengines compared to that of the normal catalytic engines with flat Pt films. The snap image is exhibited in the inset of Figure 5c. The nanoengines we chose are around 10  $\mu\text{m}$  in length. An ultrafast motion of Pt-nanoparticle-coated nanoengine in the 10%  $\text{H}_2\text{O}_2$  fuel at room temperature is shown in the video within the Supporting Information. It is calculated that the nanoengine propels at a speed of around 1950  $\mu\text{m s}^{-1}$ , which corresponds to around 195 body lengths per second. The propulsion performance of the nanoengines embedded with different Pt nanoparticles sizes (30.0 nm and 40.7 nm shown in Figure 5a) was examined in a 10%  $\text{H}_2\text{O}_2$  solution in comparison with the SiO/Cr/Pt microengines with the same length and the materials thickness but containing a 3 nm smooth inner Pt layer. The average speeds based on 20 microengines in each group are displayed in Figure 5c. One can see that a nearly four-fold acceleration can be obtained for nanoengines with  $\approx 40.7$  nm Pt nanoparticles than those with smooth Pt films. The nanoengines with smaller particles size ( $\approx 30.0$  nm) can achieve a higher acceleration and their average speed can reach up to 1630  $\mu\text{m s}^{-1}$ . Hence, nanoparticles in such catalytic tubular nanoengines provide an enhanced flux of the fuel towards Pt sites and a high surface area which can effectively boost the catalytic reaction inside the tube.

In order to evaluate the capability of speed enhancement in our nanoparticle-decorated micro-/nano-engines, we make a statistical analysis for all tubular micro/nanoengines reported in the literature. Theoretically, the average speed of the tubular microengines  $v_j^{\text{ave}}$  can be expressed by the following equation:

$$v_j^{\text{ave}} = \frac{9 m C_{\text{H}_2\text{O}_2} R_j L}{3 R_b^2 + L R_b / \left( \ln \left( \frac{2L}{R_j} \right) - 0.72 \right)} \quad (4)$$

where  $m$  is a rate constant experimentally estimated to be  $\approx 9.8 \times 10^{-4} \text{ m s}^{-1}$ .<sup>[36]</sup>  $C_{\text{H}_2\text{O}_2}$  is the concentration of  $\text{H}_2\text{O}_2$ ,  $L$  is the length of the microengines, and  $R_j$  and  $R_b$  are the radii of microengines and gaseous bubbles, respectively. To be simplified,  $R_j$  and  $R_b$  are assumed to be equal ( $R_j = R_b = R$ ), as we did in the previous investigation.<sup>[36]</sup> The expression can be further given by defining a geometrical parameter  $X = 2 L/R$ :

$$v_j^{\text{ave}} = \frac{9 m C_{\text{H}_2\text{O}_2} X}{6 + X / (\ln X - 0.72)} \quad (5)$$

The above equation suggests that the average speed of the nanoengines is mainly determined by the combined geometrical parameter  $X$  once the concentration of  $\text{H}_2\text{O}_2$  fuel is fixed. In order to show a complete image of the whole field, we plotted Equation 5 as dashed line together with results from this work (Pt-nanoparticle coated nanoengines, red column) and typical experimental data (grey squares and columns) extracted from other literatures in Figure 5d.<sup>[36–46]</sup> For the sake of clarity, we just summarized the data from micro-/nanoengines working at room temperature. The speeds are also re-calculated at a

normalized  $\text{H}_2\text{O}_2$  concentration of 5% since both Equation 4 and the previous study<sup>[36]</sup> show that the speed is nearly linear to  $\text{H}_2\text{O}_2$  concentration in a moderate range. One can see that catalytic engines in most experimental studies display the speed variation with those results predicted by Equation 5. We should stress that various fuel compositions (e.g., bio-medium or surfactant) used in the experiments may significantly influence the gas production, leading to huge deviation of  $m$  compared with the value used in our calculation. And the inevitable imperfection existed in the tubular structures may also deteriorate the dynamic interaction, decelerating the micro-/nanoengines. On the other hand, the red line corresponding to current nanoparticle-decorated nanoengines shows an obvious increase in the motion speed which can be attributed to the increased reaction activity from a large amount of dispersed catalytic nanoparticles on the inner surface of the tubular cavity. These powerful Pt-nanoparticle embedded nanoengines with fast speed and small size are highly desirable for delivery carriers within biomedical systems.

In conclusion, deterministic self-assembly, demanded in nanotechnology, needs a highly precise control of driving forces and energy minimization at the nanoscale, which has been applied in the macro-level, for example, capillary origami and 3D devices.<sup>[27–29,31]</sup> We utilize dry-releasing approach via rapid thermal annealing and manipulate the surface tension of nanodroplets to assist the rolling of strained nanomembranes, and thus push the downscale limitation of rolled-up tubes. The capillary torque generated by the nanoparticles on the nanomembrane surface can efficiently reduce the diameter of rolled-up tubes and thus overcome the downscale limitation (below 100 nm), which is consistent with our theoretical prediction. Furthermore, such small tubes embedded with Pt nanoparticles can work as nanoengines and exhibit a dramatic acceleration in speed compared to those with smooth Pt surface due to enhanced mass transfer and large surface area. Our methodology offers a great opportunity for mechanical deformation, such as folding, bending, buckling, and zipping, in nanoscale self-assembly,<sup>[2]</sup> and may enable solid nanomembranes becoming an essential building blocks in flexible electronics, and lab-on-a-chip micro/nano-electromechanical systems (MEMS/NEMS).

## Experimental Section

**Fabrication of Pattered 2D Nanomembranes on PMMA:** PMMA (5 wt% in O-xylene) was firstly spin-coated on silicon substrate. The inorganic layers were deposited on the PMMA polymer by e-beam evaporation and sputtered deposition under high vacuum ( $<10^{-4}$  Pa). Oxide ( $\text{SiO}$ ,  $\text{SiO}_2$ ,  $\text{TiO}_2$ ) films with various thicknesses of 3 nm, 5 nm, 10 nm, were deposited by e-beam evaporation. Noble metals (Au, Ag, Pt) with different thicknesses of 2 nm, 2.5 nm, and 3 nm were deposited by sputtering (ULVAC Mila-3000). A hard shadow mask containing micro square apertures was aligned on the PMMA layer during the deposition process to allow the fast patterning of nanomembranes.

**Thermal Delamination:** Soft baking of the nanomembranes/PMMA samples at 180 °C for 10 min was applied to induce the delamination of nanomembranes to form the strain-engineered tube. A detailed process of strain-engineered rolling for a twin-tube array formation was recorded by microscopy video (Supporting Information, Movie 2).

**Rapid Thermal Annealing:** Rapid thermal annealing (ULVAC ACS-4000-C4) of nanomembranes/PMMA samples was applied to generate the thermal dewetting of metal layers and release the nanomembranes. In order to tune the nanoparticles size and density, the SiO<sub>2</sub>/TiO<sub>2</sub>/Au, SiO<sub>2</sub>/TiO<sub>2</sub>/Ag, SiO<sub>2</sub>/TiO<sub>2</sub>/Pt multilayers were annealed at 400–800 °C for 10–90 s. The surface morphologies of rolled-up nanomembranes were characterized by scanning electron microscope and analyzed by the software ImageJ.

**Self-Propulsion of Nanoengines:** Rolled-up tubes consisting of Si/Cr/Pt layer and SiO<sub>2</sub>/TiO<sub>2</sub>/Pt-nanoparticle layer were placed in a 10% H<sub>2</sub>O<sub>2</sub> aqueous solution. Videos were recorded by a high-speed camera (up to 200 frames per second) connected to an optical microscopy (Olympus BX51). The real-time videos were analyzed in detail with the assistance of a particle tracking plug-in for ImageJ.

## Supporting Information

Supporting Information is available from the Wiley Online Library or from the author.

## Acknowledgements

This work is supported by the Natural Science Foundation of China (Nos. 61008029 and 51102049), Program for New Century Excellent Talents in University (No. NCET-10-0345), Shanghai Pujiang Program (No.11PJ1400900), and “Shu Guang” project by Shanghai Municipal Education Commission and Shanghai Education Development Foundation. We also thank Dr. Zhenghua An from Fudan Nano-fabrication and Devices Laboratory for experimental assistance. R.L. thanks the support from the Shanghai Education Development Foundation and the National High Technology Program (2011AA100706-2).

Received: March 15, 2013

Revised: April 12, 2013

Published online: May 24, 2013

- [1] J. A. Rogers, M. G. Lagally, R. G. Nuzzo, *Nature* **2011**, 477, 45.
- [2] G. S. Huang, Y. F. Mei, *Adv. Mater.* **2012**, 24, 2517.
- [3] V. Shenoy, D. H. Gracias, *MRS Bull.* **2012**, 37, 847.
- [4] D. H. Kim, J. A. Rogers, *ACS Nano* **2009**, 3, 498.
- [5] M. M. Roberts, L. J. Klein, D. E. Savage, K. A. Slinker, M. Friesen, G. Celler, M. A. Eriksson, M. G. Lagally, *Nat. Mater.* **2006**, 5, 388.
- [6] O. G. Schmidt, K. Eberl, *Nature* **2001**, 410, 168.
- [7] J. Yoon, S. Jo, I. S. Chun, I. Jung, H. S. Kim, M. Meitl, E. Menard, X. Li, J. J. Coleman, U. Paik, J. A. Rogers, *Nature* **2010**, 465, 329.
- [8] H. X. Ji, X. L. Wu, L. Z. Fan, C. Krien, I. Fiering, Y. G. Guo, Y. F. Mei, O. G. Schmidt, *Adv. Mater.* **2010**, 22, 4591.
- [9] J. Wang, T. R. Zhan, G. S. Huang, X. G. Cui, X. H. Hu, Y. F. Mei, *Opt. Express* **2012**, 20, 18555.
- [10] E. J. Smith, Z. W. Liu, Y. F. Mei, O. G. Schmidt, *Nano Lett.* **2010**, 10, 1.
- [11] M. Jamal, A. M. Zarafshar, D. H. Gracias, *Nat. Commun.* **2011**, 2, 1.
- [12] S. M. Harazim, V. A. B. Quiñones, S. Kiravittaya, S. Sanchez, O. G. Schmidt, *Lab Chip* **2012**, 12, 2649.
- [13] Y. F. Mei, A. A. Solovev, S. Sanchez, O. G. Schmidt, *Chem. Soc. Rev.* **2011**, 40, 2109.
- [14] A. A. Solovev, W. Xi, D. H. Gracias, S. Harazim, C. Deneke, S. Sanchez, O. G. Schmidt, *ACS Nano* **2012**, 6, 1751.
- [15] R. J. Ellis, S. M. Vandervies, *Annu. Rev. Biochem.* **1991**, 60, 321.
- [16] J. Wang, *Analytical Electrochemistry*, 3rd ed., Wiley, New York **2006**.
- [17] Y. W. Lu, C. J. Kim, *Appl. Phys. Lett.* **2006**, 89, 164101.
- [18] Y. P. Hsieh, Z. H. Wei, *Jpn. J. Appl. Phys.* **2011**, 50, 037203.
- [19] J. K. Luo, R. Huang, J. H. He, Y. Q. Fu, A. J. Flewitt, S. M. Spearing, N. A. Fleck, W. I. Milne, *Sens. Actuators, A* **2006**, 132, 346.
- [20] J. C. Nawroth, H. Lee, A. W. Feinberg, C. M. Ripplinger, M. L. McCain, A. Grosberg, J. O. Dabiri, K. K. Parker, *Nat. Biotechnol.* **2012**, 30, 792.
- [21] M. H. Huang, C. Boone, M. Roberts, D. E. Savage, M. G. Lagally, N. Shaji, H. Qin, R. Blick, J. A. Nairn, F. Liu, *Adv. Mater.* **2005**, 17, 2860.
- [22] Y. F. Mei, G. S. Huang, A. A. Solovev, E. B. Ureña, I. Mönch, F. Ding, T. Reindl, K. Y. Fu, P. K. Chu, O. G. Schmidt, *Adv. Mater.* **2008**, 20, 4085.
- [23] J. H. Cho, T. James, D. H. Gracias, *Adv. Mater.* **2010**, 22, 2320.
- [24] J.-H. Cho, D. Datta, S.-Y. Park, V. B. Shenoy, D. H. Gracias, *Nano Lett.* **2010**, 10, 5098.
- [25] H. K. Pulker, *Thin Solid Films* **1982**, 89, 191.
- [26] S. Sanchez, A. A. Solovev, S. M. Harazim, C. Deneke, Y. F. Mei, O. G. Schmidt, *Chem. Rec.* **2011**, 11, 367.
- [27] C. Py, P. Reverdy, L. Doppler, J. Bico, B. Roman, C. N. Baroud, *Phys. Rev. Lett.* **2007**, 98, 156103.
- [28] L. Q. Chen, X. Wang, W. J. Wen, Z. G. Li, *Appl. Phys. Lett.* **2010**, 97, 124103.
- [29] C. Y. Guo, H. Lic, B. Y. Ahna, E. B. Duossa, K. J. Hsiao, J. A. Lewis, R. G. Nuzzo, *Proc. Natl. Acad. Sci. USA* **2009**, 106, 20149.
- [30] N. Patra, B. Y. Wang, P. Král, *Nano Lett.* **2009**, 9, 3766.
- [31] J. S. Huang, M. Juskiewicz, W. H. Jeu, E. Cerda, T. Emrick, N. Menon, T. P. Russell, *Science* **2007**, 317, 650.
- [32] L. D. Landau, E. M. Lifshitz, *Theory of Elasticity*, 3rd ed., Pergamon Press, Oxford **1986**.
- [33] A. A. Solovev, S. Sanchez, M. Pumera, Y. F. Mei, O. G. Schmidt, *Adv. Funct. Mater.* **2010**, 20, 2430.
- [34] S. Campuzano, J. Orozco, D. Kagan, M. Guix, W. Gao, S. Sattayasamitsathit, J. C. Claussen, A. Merkoçi, J. Wang, *Nano Lett.* **2011**, 12, 396.
- [35] J. Wang, W. Gao, *ACS Nano* **2012**, 6, 5745.
- [36] J. X. Li, G. S. Huang, M. M. Ye, M. L. Li, R. Liu, Y. F. Mei, *Nanoscale* **2011**, 3, 5083.
- [37] A. A. Solovev, Y. F. Mei, E. B. Ureña, G. S. Huang, O. G. Schmidt, *Small* **2009**, 5, 1688.
- [38] W. Gao, S. Sattayasamitsathit, J. Orozco, J. Wang, *J. Am. Chem. Soc.* **2011**, 133, 11862.
- [39] G. S. Huang, J. Wang, Y. F. Mei, *J. Mater. Chem.* **2012**, 22, 6519.
- [40] J. Orozco, S. Campuzano, D. Kagan, M. Zhou, W. Gao, J. Wang, *Anal. Chem.* **2011**, 20, 7962.
- [41] K. M. Manesh, M. Cardona, R. Yuan, M. Clark, D. Kagan, S. Balasubramanian, J. Wang, *ACS Nano* **2010**, 4, 1799.
- [42] S. Sanchez, A. N. Ananth, V. M. Fomin, M. Viehrig, O. G. Schmidt, *J. Am. Chem. Soc.* **2011**, 38, 14860.
- [43] A. A. Solovev, E. J. Smith, C. C. B. Bufon, S. Sanchez, O. G. Schmidt, *Angew. Chem. Int. Ed.* **2011**, 46, 10875.
- [44] Z. Q. Liu, J. X. Li, J. Wang, G. S. Huang, R. Liu, Y. F. Mei, *Nanoscale* **2012**, 5, 1345.
- [45] S. Sanchez, A. A. Solovev, S. Schulze, O. G. Schmidt, *Chem. Commun.* **2011**, 47, 698.
- [46] M. Guix, J. Orozco, M. García, W. Gao, S. Sattayasamitsathit, A. Merkoçi, A. Escarpa, J. Wang, *ACS Nano* **2012**, 5, 4445.